


Climate and landform interact to control the source and transport of nitrate in Pacific Northwest rivers

Elizabeth J. Elmstrom ^{1✉}, Gordon W. Holtgrieve ¹, Mark D. Scheuerell^{1,2}, Andrew J. Schauer³ & Karrin Leazer⁴

The hydrological effects of climate change are documented in many regions; however, climate-driven impacts to the source and transport of river nutrients remain poorly understood. Understanding the factors controlling nutrient dynamics across river systems is critical to preserve ecosystem function yet challenging given the complexity of landscape and climate interactions. Here, we harness a large regional dataset of nitrate (NO_3^-) yield, concentration, and isotopic composition ($\delta^{15}\text{N}$ and $\delta^{18}\text{O}$) to evaluate the strength of hydroclimate and landscape variables in controlling the seasonal source and transport of NO_3^- . We show that hydroclimate strongly influenced the seasonality of river NO_3^- , producing distinct, source-dependent NO_3^- regimes across rivers from two mountain ranges. Riverine responses to hydroclimate were also constrained by watershed-scale topographic features, demonstrating that while regional climate strongly influences the timing of river NO_3^- transport, watershed topography plays a distinct role in mediating the sensitivity of river NO_3^- dynamics to future change.

¹School of Aquatic and Fishery Sciences, University of Washington, Seattle, WA, USA. ²U.S. Geological Survey Washington Cooperative Fish and Wildlife Research Unit, School of Aquatic and Fishery Sciences, University of Washington, Seattle, WA, USA. ³Department of Earth and Space Sciences and IsoLab, University of Washington, Seattle, WA, USA. ⁴Department of Environmental Sciences, Western Washington University, Bellingham, WA, USA. ✉email: elmstrom@uw.edu

Rivers and streams play a critical role in regional nitrogen (N) cycles through the transport and in situ processing of dissolved reactive N as it moves from the land to the coast¹. Dramatic increases in the load of N to freshwaters from human activities have stressed the bounds of riverine N processes, fundamentally altering patterns of riverine N transport, and exacerbating eutrophication in freshwaters and estuaries^{2–4}. Despite substantial investment to reduce watershed N loads to rivers, anthropogenic activity and land use change continue to elevate N sources across the landscape⁵. Furthermore, as climate change strengthens precipitation patterns, hydroclimatic shifts are projected to alter the seasonal timing and delivery of NO_3^- (frequently the dominant form of dissolved N) from watersheds to rivers and streams⁶. Understanding the factors controlling seasonal river NO_3^- variation is critical to evaluate impacts downstream, but the balance of landscape and hydroclimatic variables in driving the N export dynamic remains unclear.

For any river system, landscape features represent a potentially dominant driver of instream NO_3^- concentrations and NO_3^- yields^{7–11}. Specifically, geomorphic attributes, such as watershed slope, channel morphology, and floodplain area, determine water residence times and hydrologic connectivity, ultimately governing watershed NO_3^- retention, loss (via biotic uptake or denitrification), and movement from watersheds to rivers and streams^{9–13}. Such catchment characteristics also influence the source composition and availability of NO_3^- by determining the structure and composition of vegetation and soils, and by constraining the spatial distribution of human activity. In watersheds with steep slopes, catchment topography limits human activity, restricting NO_3^- source composition to nitrified soil ammonium (NH_4^+) and atmospheric deposition^{14,15}. Lower sloped areas instead increase space for human development, agricultural activity, and the growth of N-fixing species (such as alders, *Alnus* spp.)¹⁵, promoting the accumulation of N in soils and groundwater, enhancing the transport potential of NO_3^- ^{16,17}. Spatial and temporal variation of river NO_3^- is further controlled by seasonal precipitation patterns and river flow, which mobilize NO_3^- from the landscape and drive the timing and magnitude of NO_3^- transport across systems^{18,19}.

Characterizing how different landscape and hydroclimatic controls transport or retain nutrients is important to improve the understanding of future river NO_3^- exports, but difficult due to the multiple scales at which drivers operate and the complex interactions they produce^{20–22}. For instance, current ecological stressors, such as changing land use and climate change, are global in scale with impacts that propagate differently across ecosystems^{19,23}. In riverine environments, climate-induced shifts to the quantity and form (rain vs. snow) of precipitation will alter the timing and magnitude of river discharge. Specifically, in northern latitudes like the Pacific Northwest, increases in flashy, event-driven runoff and decreases in spring snowmelt are projected to substantially alter seasonal hydrologic regimes^{24,25}. The integration of landscape-level features, such as watershed slope or past land use histories, within these larger patterns will likely produce different ecosystem responses, making local variations of river NO_3^- exports difficult to predict^{23,26,27}. The interaction of complex landscapes with altered climate patterns and river flows thus represents a key uncertainty in our understanding of riverine responses to ongoing climate and land use change.

While the impact of large-scale stressors may manifest differently in rivers and streams, precipitation and river flow have been shown to synchronize seasonal patterns of river NO_3^- concentration and yield across watersheds that share similar characteristics^{28,29}. Flow-dependent nutrient regimes at the seasonal scale have been revealed, most recently in the Great Lakes, where monthly NO_3^- concentrations were shown to be

synchronous with discharge in both agricultural and unmanaged catchments²⁸. Urban streams instead exhibited high concentrations during summer low-flow periods, creating out-of-phase nutrient regimes. In mountainous landscapes, research has shown that the physical features of watersheds can act as master controls of physiochemical^{23,26,30,31} and biological processes³², and constrain the susceptibility of ecosystem responses to climate and hydrologic variation. Such relationships highlight the importance of hydrologic connections and the role of both regional and local scale drivers (e.g., climate, land use, and geomorphology) in the N export dynamic, and support the notion that by evaluating temporal patterns across rivers subject to different controls, we can better understand the underlying processes that generate patterns over space and time^{20,22,33}.

Increasingly applied over the past decades, the stable isotopes of NO_3^- ($\delta^{15}\text{N}$ and $\delta^{18}\text{O}$) are tracers of N sources and biogeochemical transformations, with potential to unravel larger spatiotemporal trends³⁴. Traditional applications of dual isotopic studies have focused on source identification using $\delta^{15}\text{N}$ and $\delta^{18}\text{O}$ biplots, however overlapping ranges of $\delta^{15}\text{N}$ and $\delta^{18}\text{O}$ of NO_3^- source values often limit direct source apportionment^{14,15,35}. This overlap is further confounded by soil, aquifer, and stream processes (nitrification, denitrification, and assimilation) that fractionate $\delta^{15}\text{N}$ and $\delta^{18}\text{O}$ of NO_3^- values and alter isotopic signatures of NO_3^- pools^{34–36}. Despite uncertainties in the assessment of sources, there is growing isotopic evidence that river NO_3^- concentrations are driven by hydrologic connections with different ecosystem compartments (e.g., direct water transfer through soils during storms events, groundwater inputs, or hyporheic exchange)^{35,37–40}. This has been shown in both temperate and tropical watersheds, where, at high river stages, NO_3^- concentrations have been isotopically linked to the transfer of soil N from the legacy of human activity or from forest organic matter^{35,37–41}. Inputs from atmospheric NO_3^- are also linked to the hydrograph and have been shown to increase with spring and summer snowmelt in watersheds with higher elevation areas^{14,42}. This suggests that instream $\delta^{15}\text{N}\text{-NO}_3^-$ and $\delta^{18}\text{O}\text{-NO}_3^-$ values more accurately represent a mixture of seasonally dependent N-sources and fractionations, the proportions of which largely depend on the land use history, geomorphology, and hydrographic stage of the catchment.

Whether seasonal NO_3^- dynamics are spatially coherent among rivers can help reveal the drivers of N sources and exports; however, the evaluation of seasonal patterns across river $\delta^{15}\text{N}$ and $\delta^{18}\text{O}$ of NO_3^- time series has yet to be explored as an isotopic tool. Here, we took advantage of a unique two-year monthly data set of NO_3^- concentration and yield, combined with corresponding sample analysis of dual-isotopes of NO_3^- ($\delta^{15}\text{N}$, and $\delta^{18}\text{O}$) from 13 rivers that drain the Puget Sound basin in Washington State (see Fig. 1 for sample sites, see Fig. 2 for measured values). We applied a series of multivariate autoregressive state space models to quantify the degree to which monthly patterns of NO_3^- yield, NO_3^- concentration, $\delta^{15}\text{N}\text{-NO}_3^-$, and $\delta^{18}\text{O}\text{-NO}_3^-$ (and therefore the inferred source of NO_3^-) were coherent across the basin. Through the inclusion of environmental covariates, we then characterized potential hydroclimate drivers shaping the timing, direction, and magnitude of monthly river NO_3^- dynamics, and quantified how their effects varied across systems. We aim to address three questions: (1) Are there shared monthly patterns in river NO_3^- yield, NO_3^- concentration, $\delta^{15}\text{N}\text{-NO}_3^-$, and $\delta^{18}\text{O}\text{-NO}_3^-$ across Puget Sound rivers, and, if so, at what spatial or functional scale? (e.g., entire Puget Sound basin, among mountain ranges, or among land use or geomorphic groupings, Table 1), (2) What climate and hydrologic variables are best related to monthly variation in river NO_3^- yield, NO_3^- concentration, $\delta^{15}\text{N}\text{-NO}_3^-$, and

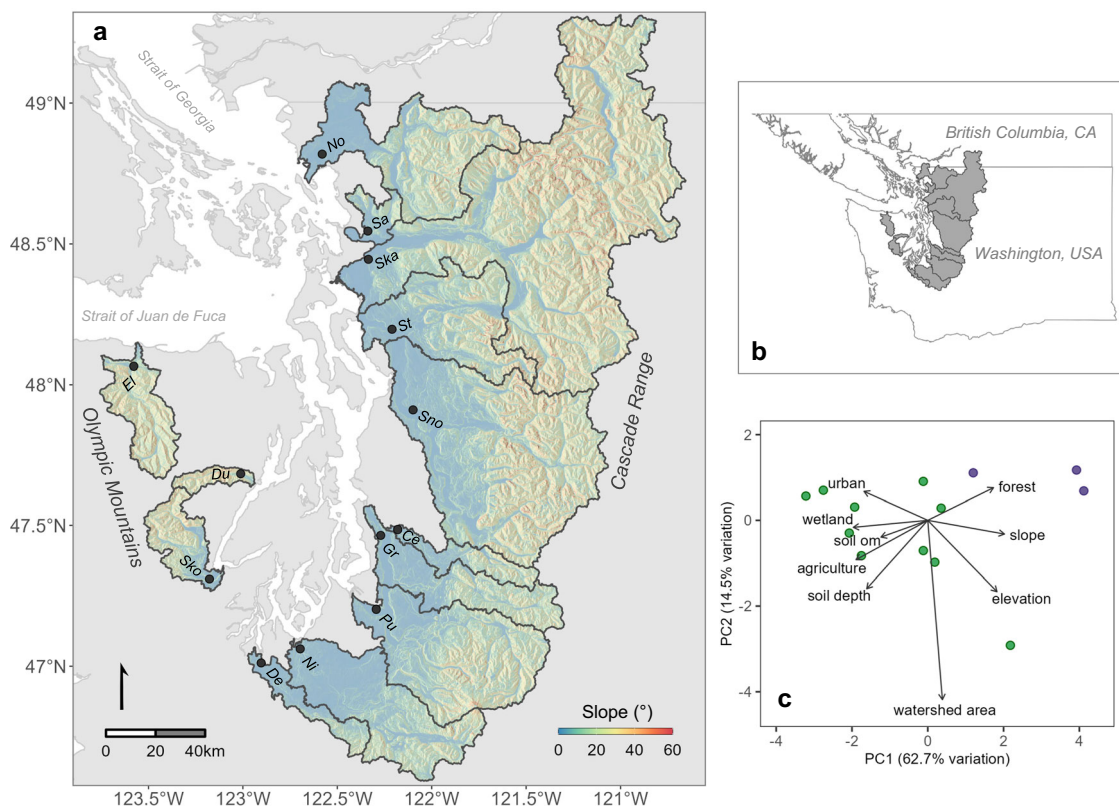


Fig. 1 Map and characteristics of the Puget Sound Basin watersheds of study. **a** The watersheds of study shaded with their local slope in degrees. Black points represent the river water quality sampling stations. Italicized abbreviations refer to the river names, which are provided in full in Table 2. **b** Location of the Puget Sound Basin within Washington state and British Columbia. **c** Ordination plot showing principal component analysis (PCA) of watershed characteristics from the Puget Sound Basin rivers. Green points represent rivers located in the Cascade Mountains. Purple points represent rivers located in the Olympic Mountains. Length and direction of arrows on the ordination are proportional to vector loading of watershed characteristics into each principal component (PC).

$\delta^{18}\text{O}-\text{NO}_3^-$, and (3) How does the response of river NO_3^- yield, NO_3^- concentration, $\delta^{15}\text{N}-\text{NO}_3^-$ and $\delta^{18}\text{O}-\text{NO}_3^-$ to hydroclimate variables vary with watershed-specific characteristics? By summarizing monthly variation at this regional scale, we sought to gain a better understanding of whether regional controls (like climate or hydrology), or individual watershed variation (land-use or geomorphic traits) played a larger role in driving seasonal patterns of yield, concentration, and source of river NO_3^- . Further, by looking at the individual river responses to hydroclimate variation, we sought to understand how the sensitivity of seasonal NO_3^- dynamics to hydroclimatic change might be modified by watershed-specific features, such as land use cover, soil characteristics, or watershed slope.

Results

Shared monthly patterns in river NO_3^- dynamics. We found that temporal patterns in monthly river NO_3^- dynamics were strongly coherent across the Puget Sound basin at the mountain range scale. For all four response variables (NO_3^- yield, NO_3^- concentration, $\delta^{15}\text{N}-\text{NO}_3^-$, and $\delta^{18}\text{O}-\text{NO}_3^-$), the model with states defined by mountain range resulted in the greatest support compared to either individual watershed, or land use, geomorphology, and basin-wide grouping structures (Supplementary Tables 1–4). The next best model in terms of river grouping was the geomorphology grouping structure, which was also consistent across all four response variables. However, none of the geomorphology models had particularly high statistical support ($\Delta\text{AICc} < 2$), with ΔAICc s of 8.7, 3.2, 8.3, and 9.3 for NO_3^- yield, NO_3^- concentration, $\delta^{15}\text{N}-\text{NO}_3^-$, and $\delta^{18}\text{O}-\text{NO}_3^-$, respectively.

This suggests that monthly variation in NO_3^- yield, NO_3^- concentration, $\delta^{15}\text{N}-\text{NO}_3^-$, and $\delta^{18}\text{O}-\text{NO}_3^-$ was best defined by two river state processes, one for rivers located in the Cascade Range, and one for rivers located in the Olympic Mountains (Fig. 3).

Models with correlated process errors were best supported by all response variable data (Supplementary Tables 1–4). For NO_3^- yield, NO_3^- concentration, and $\delta^{18}\text{O}-\text{NO}_3^-$, the best process error structure had equal variance and covariance among the two state processes (Supplementary Tables 1, 2, and 4), indicating that states across the two mountain ranges were temporally correlated and shared similar magnitudes in the peaks and troughs of their curves through time. For $\delta^{15}\text{N}-\text{NO}_3^-$, the best model included an unconstrained **Q** matrix structure (Supplementary Table 3), indicating that states were temporally correlated across mountain ranges, but the magnitude of monthly variation differed between the Cascade Range and Olympic Mountain rivers.

Hydroclimate drivers of monthly river NO_3^- variation. For all response variables, the best covariate model included a shared coefficient among rivers within each mountain range (Supplementary Tables 5–8). That is, rivers in the Cascade Range shared similar effects of hydroclimate variables, while the effects of hydroclimate variables shared by rivers in the Olympic Mountains were distinctly different. For example, for both NO_3^- yield and concentration, the model including precipitation had the most data support (Supplementary Tables 5–6), but the magnitude and directionality of the precipitation effect varied for rivers in each mountain range. In the Cascade Range rivers, precipitation had a positive effect on NO_3^- concentration and yield

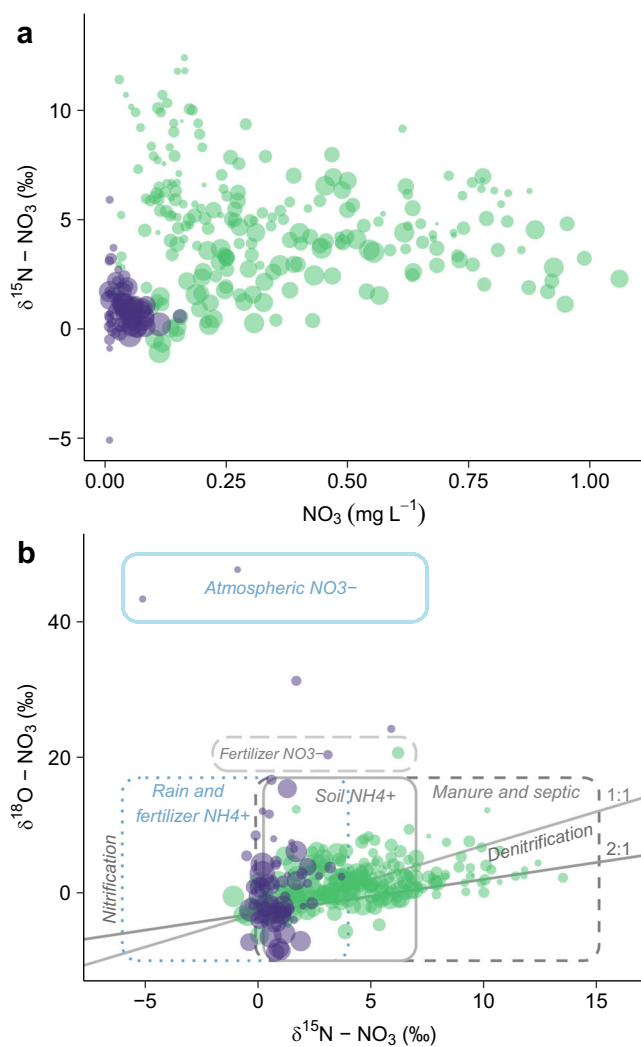


Fig. 2 NO_3^- concentrations, $\delta^{15}\text{N-NO}_3^-$, and $\delta^{18}\text{O-NO}_3^-$ measured in the Puget Sound rivers. **a** $\delta^{15}\text{N-NO}_3^-$ plotted versus NO_3^- concentrations. **b** $\delta^{18}\text{O-NO}_3^-$ plotted versus $\delta^{15}\text{N-NO}_3^-$. Green points are values measured in the Cascade Range rivers. Purple points are values measured in the Olympic Mountain rivers. Symbol size corresponds to the amount of precipitation (mm) that fell during the month when sample was taken. Typical ranges of the different nitrate end-members are also presented¹⁵, as well as the two typical trends (1:1 and 2:1) observed in literature¹⁵ for denitrification.

(Fig. 4a, b), indicating that during periods of heavy rainfall, the amount and export of river NO_3^- increased. In the Olympic Mountain rivers, however, precipitation's effect on NO_3^- yield was smaller than rivers in the Cascade Range, and the effect on river NO_3^- concentrations was strongly negative (though not statistically significant from 0, Fig. 4a, b). For both NO_3^- concentration and yield, the next best covariate model included an effect of water temperature at the mountain range scale (NO_3^- concentration $\Delta\text{AIC}_c = 1.9$, NO_3^- yield $\Delta\text{AIC}_c = 9.8$). In the Cascade Range rivers, water temperature had a negative effect on NO_3^- yield but was unrelated to NO_3^- concentrations. Conversely, in the Olympic Mountain rivers, the effect of water temperature was unrelated to NO_3^- yields but exhibited a strong positive effect on NO_3^- concentrations (Fig. 4a, b).

Event-scale discharge and precipitation best explained variation across $\delta^{15}\text{N-NO}_3^-$ patterns (Q_{quick} $\Delta\text{AIC}_c = 0$, Precipitation $\Delta\text{AIC}_c = 6.7$, Supplementary Table 7). In the Cascade Range rivers, Q_{quick} had a strong, negative effect on the $\delta^{15}\text{N-NO}_3^-$

time series (Fig. 4c), indicating that depleted $\delta^{15}\text{N-NO}_3^-$ values were highly correlated with winter runoff or storm events. The effect of Q_{quick} on $\delta^{15}\text{N-NO}_3^-$ was, however, not present in the Olympic Mountain rivers, as indicated by an effect size that was not statistically distinguishable from 0 (Fig. 4c). Precipitation was the second-best explanatory covariate for $\delta^{15}\text{N-NO}_3^-$ and further enforced these differences between the two mountain ranges. In the Cascade Range rivers, $\delta^{15}\text{N-NO}_3^-$ values decreased when precipitation increased (Fig. 4c), and again, in the Olympic Mountain rivers the effect of precipitation on $\delta^{15}\text{N-NO}_3^-$ was not statistically distinguishable from 0 (Fig. 4c).

For $\delta^{18}\text{O-NO}_3^-$, snowmelt was the best descriptor of isotopic variation (Supplementary Table 8). Snowmelt had a strong, positive effect on $\delta^{18}\text{O-NO}_3^-$ in the Olympic Mountain rivers (Fig. 4d), but no effect on $\delta^{18}\text{O-NO}_3^-$ in rivers in the Cascade Range (Fig. 4d). The second most parsimonious model for $\delta^{18}\text{O-NO}_3^-$ at the mountain range scale included Q_{quick} ($\Delta\text{AIC}_c = 7.7$). Positive values of Q_{quick} were strongly related to depleted $\delta^{18}\text{O-NO}_3^-$ values in the Cascade Range (negative effect sizes, Fig. 4d). In the Olympic Mountain rivers, Q_{quick} had a positive, but insignificant, effect (Fig. 4d).

For all response variables, no other explanatory covariate had a high ($\Delta\text{AIC}_c < 2$) or moderate ($\Delta\text{AIC}_c < 10$) degree of support. However, the second most parsimonious model for all the best explanatory covariate models included a common response to hydroclimate at the geomorphic grouping scale (Supplementary Tables 5–8).

Landscape controls of river NO_3^- responses to hydroclimate.

The sensitivity of NO_3^- , NO_3^- yield, $\delta^{15}\text{N-NO}_3^-$, and $\delta^{18}\text{O-NO}_3^-$ among rivers to hydroclimate drivers (i.e., covariate effect sizes) covaried strongly with mean watershed slope (Fig. 5). For both NO_3^- concentration and yield, steeper watersheds were less sensitive to the positive effects of precipitation. As mean watershed slope increased, the effect of precipitation on NO_3^- yield diminished (Fig. 5a) or became negative for NO_3^- concentration (Fig. 5b). Similarly, the negative effect of Q_{quick} on $\delta^{15}\text{N-NO}_3^-$ was greater in rivers draining relatively flat watersheds with more floodplain area and the effect lessened as watershed slope increased (Fig. 5c). Rivers draining steeper watersheds had the strongest effect of snowmelt on $\delta^{18}\text{O-NO}_3^-$, and this effect did not exist or was negative in less-steep watersheds (Fig. 5d).

Discussion

Using a unique regional dataset, we show the monthly riverine NO_3^- dynamics were coherent across watersheds within individual mountain ranges, despite wide variation in land use and hydrologic regimes across watersheds in the Puget Sound Basin. Our findings demonstrate the overarching importance of regional-scale climate drivers such as precipitation on N transport in rivers, while simultaneously identifying different components of the hydrograph as an important control of monthly NO_3^- source variation in both human-influenced and in more pristine catchments. Furthermore, we found that not all rivers were equally sensitive to hydroclimate variables, and that variation in this sensitivity was largely determined by a simple geomorphic feature - mean watershed slope. These results suggest that while regional-scale climate controls seasonal NO_3^- delivery in Puget Sound rivers, watershed topography plays a distinct role in influencing landscape-level drivers of NO_3^- source and transfer, which together modify the response of riverine NO_3^- dynamics to hydroclimatic change.

Seasonal patterns at the mountain-range scale. Monthly coherence in NO_3^- dynamics at the mountain-range scale

Table 1 Description model structures considered in the MARSS time series models.

Model name	Model descriptions	# of state processes
Basin	All rivers in the Puget Sound basin follow the same hidden state or trend through time	1
Mountain	There are two hidden states defined by mountain range, one for rivers located in the Cascade Range, and one for rivers located in Olympic Mountains	2
Land use	Rivers that share similar watershed land use and degree of human disturbance follow the same hidden state (i.e., urban vs. agriculture vs. forest)	3
Geomorphology	Rivers that share similar watershed topographic and soil characteristics follow the same hidden state. Groupings as follows: (1) Small watershed area, high slope and elevation, lower soil depths and organic matter (OM), (2) Large watershed area, high slope and elevation, lower soil depths and OM, (3) Intermediate watershed area, lower slope and elevation, and higher soil depths and OM	3
Watershed	Each river follows its own independent state or trend through time	13

Models compared groupings of NO_3^- concentration, NO_3^- yield, $\delta^{15}\text{N}$, and $\delta^{18}\text{O}$ of NO_3^- time series and the effects of hydroclimate on state processes at different spatial and functional scales (see “Methods” for details).

suggests that regional-scale processes have stronger controls on seasonal patterns of NO_3^- concentration, yield, and isotopic signatures than finer watershed-scale variation. Given known links between river discharge, solute concentration, and flux^{19,28,29}, we anticipated some degree of coherence in NO_3^- concentration and yield time series among rivers, but the exact extent of that coherence was unknown. The separation of NO_3^- yield and NO_3^- concentration patterns in the Cascade Range and Olympic Mountain rivers likely reflects the cumulative differences in landscape composition that exist between the two mountain ranges. The lower sloped watersheds of the Cascade Range have sprawling valley floors, with larger wetland and riparian areas, deeper soils, and varied degrees of agricultural activity and human development. Watersheds in the Olympic Mountains are instead spatially constrained in relief, generally high elevation, and remain mostly forested with little to no agriculture and sparse human development (Table 2 and Fig. 1c). Our results thus agree with previous work that seasonal-scale nutrient regime curves can be driven by regional-scale variation, such as seasonal flow and precipitation patterns, but become asynchronous with varying physical traits and land use histories due to differences in source type and availability²⁸.

With large variation in watershed land use and hydrogeomorphic characteristics among the Puget Sound basin rivers (Table 2 and Fig. 1c), we expected watershed-specific traits to drive varied source proportions and processing rates and to diminish the coherence in monthly values of $\delta^{15}\text{N}$ and $\delta^{18}\text{O}$ of NO_3^- . Instead, despite broad variation in watershed characteristics, rivers in the Cascade Range experienced notable coherence $\delta^{15}\text{N}$ - NO_3^- and $\delta^{18}\text{O}$ - NO_3^- over time, and rivers in the Olympic Mountains shared strong monthly patterns of $\delta^{18}\text{O}$ - NO_3^- , but little change in $\delta^{15}\text{N}$ - NO_3^- (Fig. 3). The observed degree of coherence found across $\delta^{15}\text{N}$ and $\delta^{18}\text{O}$ of NO_3^- time series, along with the divergent patterns between the Cascade Range and Olympic Mountain rivers, suggests that the two isotopic states depict a region-specific mixture of seasonally dependent NO_3^- sources, or perhaps show cumulative fractionation processes that are similar in each river group.

Hydroclimate drivers in the Cascade Range and Olympic Mountain rivers. The support for seasonal coherence at the mountain range scale was further corroborated by our covariate analysis, where correlations between hydroclimate drivers and NO_3^- response variables highlighted fundamental differences in NO_3^- source availability, transport potential, and transformation processes across the Cascade Range and Olympic Mountains. In the Cascade Range rivers, we found that precipitation had positive effects on both NO_3^- concentration and yield, and that NO_3^-

yields decreased seasonally as the hydrograph fell and river waters warmed (as indicated by the negative effect of water temperature; Fig. 4a). This finding supports the notion that in these moderately to highly disturbed catchments, river nutrient export is “transport limited”, and that NO_3^- yields are primarily driven by the seasonal mobilization of NO_3^- sources with increased precipitation and resultant river flow^{19,29}. In anthropogenically modified watersheds, N accumulates within soils and groundwater from fertilizer and manure applications^{16,29}, septic waste^{43,44}, N-fixing species (such as legumes or alder^{18,45}), or from altered atmospheric deposition patterns across the watershed^{14,42,46}. Consistent relationships between hydroclimate variables and NO_3^- loads across human-modified catchments have thus been attributed to the mobilization of accumulated NO_3^- pools in soils and groundwater^{16,29}, rather than direct runoff from surface point sources.

In the Olympic Mountain rivers, the effect of precipitation on NO_3^- yield was positive, but smaller than in the Cascade Range rivers, signaling a reduced response of monthly NO_3^- transport to increased precipitation in rivers draining relatively intact watersheds. Snowmelt had a negative effect on NO_3^- yields in Olympic Mountain rivers, which reflects a decrease in NO_3^- export during spring freshets in rivers with snow-driven hydrologies. This, combined with the uniformly negative effects of hydroclimate variables on NO_3^- concentrations, suggests that Olympic Mountain rivers were highly sensitive to the effects of seasonal dilution with increased river volume. Negative concentration-discharge relationships have been shown in other forested and undeveloped watersheds^{47,48}, and have been described as “source limited” due to the absence of excess watershed N supplies. In these systems, NO_3^- concentrations peak in the summer and during the rising limb of the hydrograph from increased stream or nearby soil nitrification pools, then decrease with the exhaustion of sources⁴⁷. The increase in NO_3^- concentrations with warm summer flows supports this hypothesis (positive effect of water temperature; Fig. 4b). Collectively, this indicates that the Olympic Mountain rivers are “source limited” in their NO_3^- patterns and that NO_3^- source pools are quickly depleted with the onset of fall precipitation.

Our isotopic results reinforce this distinction between “transport” and “source limited” NO_3^- regimes in the Cascade Range and Olympic Mountain rivers and highlight the importance of hydrologic connections between different ecosystem compartments, such as soil N pools. After the addition from fertilizers, atmospheric deposition, snowmelt, or mineralization within soils, NH_4 can be nitrified to NO_3^- , resulting in high NO_3^- concentrations with relatively low $\delta^{15}\text{N}$ - NO_3^- and $\delta^{18}\text{O}$ - NO_3^- values^{15,35–37,49}. This is especially relevant in watersheds with historical and current land use change, where additions of N to

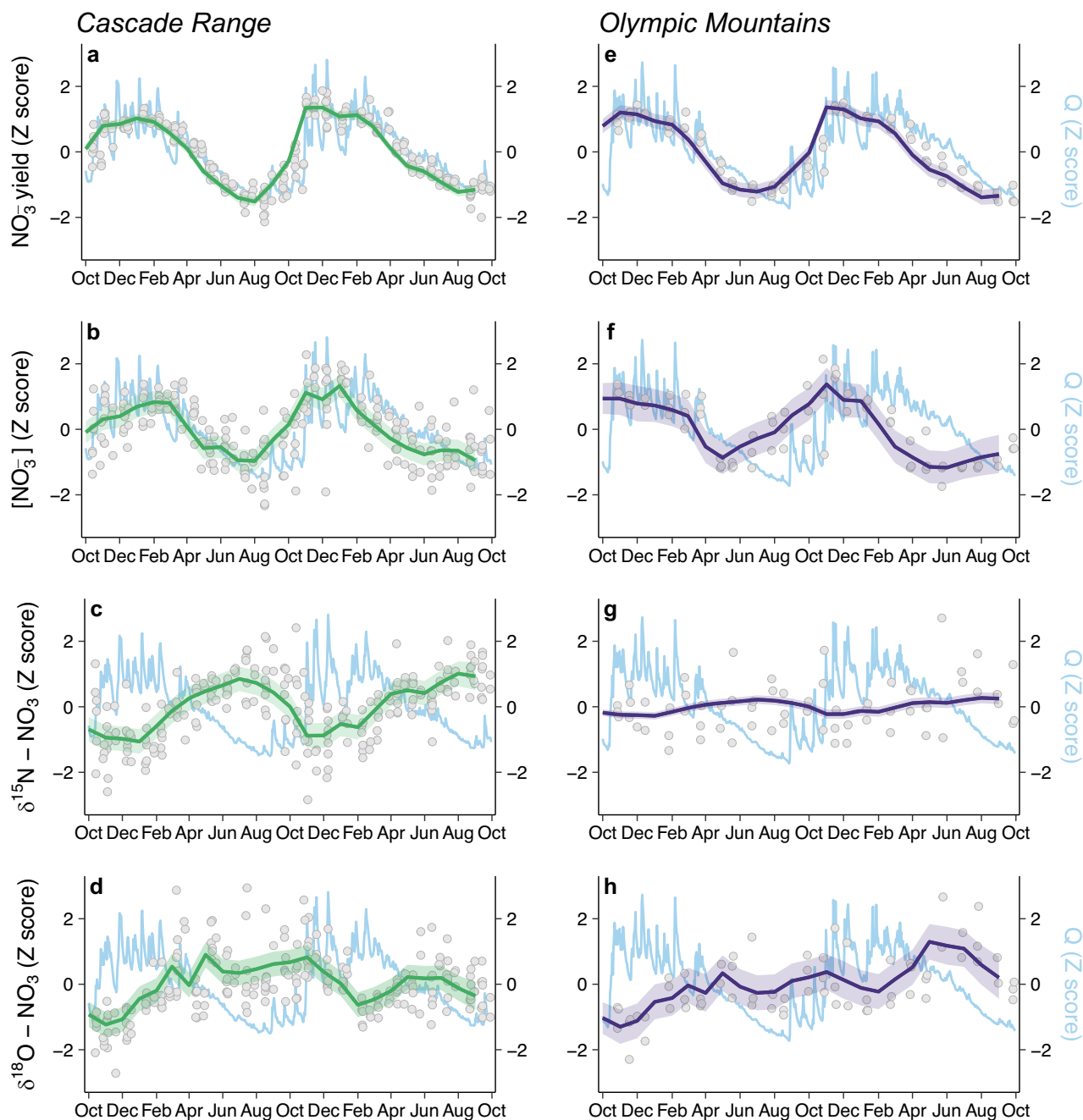


Fig. 3 Modeled states for each response variable at the “Mountain range” scale (our most supported model). Green lines are the Cascade-level modeled state for each response variable (a–d). Purple lines are the Olympic-level modeled state for each response variable (e–h). Estimates are shown with their standard error, shaded in green and purple respectively. Gray circles represent the measured water quality sample data for the individual watersheds. Blue lines represent mean daily discharge across each mountain range river group. All data are standardized by mean and variance.

the landscape enhance soil mineralization and subsequent nitrification rates⁵⁰. Higher net nitrification has also been shown to occur under N-fixing red alder trees^{51,52}, a species prevalent along the Cascade Range valley floors due to both human and riparian disturbance. In the Cascade Range rivers, the observed negative relationship between storm event-scale variations in river flow (Q_{quick}) and precipitation and $\delta^{15}\text{N}-\text{NO}_3^-$ thus implies that heavy winter rains and flooding may uniformly and rapidly mobilize nitrified soil NH_4^+ , decreasing river $\delta^{15}\text{N}-\text{NO}_3^-$ during high flow events. The decrease in river $\delta^{15}\text{N}-\text{NO}_3^-$ with winter

rains could also be attributed to the delivery of atmospheric NO_3^- or direct runoff from NO_3^- -based fertilizers. However, if that were the case, $\delta^{18}\text{O}-\text{NO}_3^-$ would have increased with precipitation. Instead, Cascade Range $\delta^{18}\text{O}-\text{NO}_3^-$ values decreased with increased event-scale flow and precipitation (negative effect sizes; Fig. 4), supporting a link between wintertime NO_3^- yields and inputs of nitrified soil NH_4^+ from the legacy of human activity in the region.

The Cascade Range rivers experienced noticeable enrichment of $\delta^{15}\text{N}-\text{NO}_3^-$ during the spring and summer months as NO_3^-

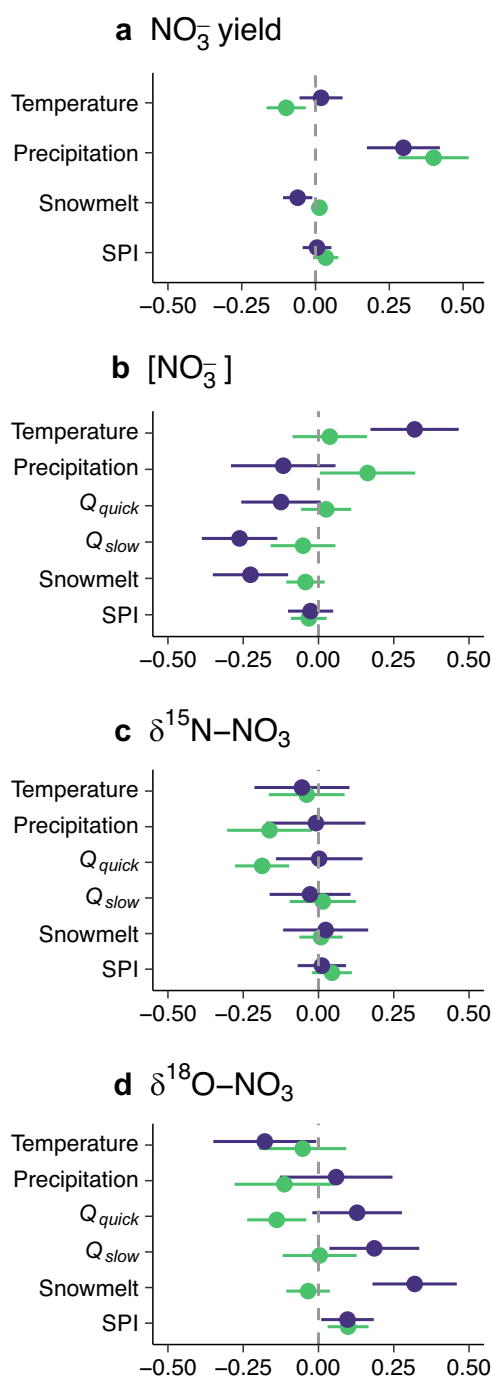


Fig. 4 Estimated MARSS model coefficients for each covariate model considered at the mountain range scale. **a** Effects of water temperature, precipitation, snowmelt and Standardized Precipitation Index (SPI) on NO_3^- yield at the mountain range scale. **b–d** Effects of water temperature, precipitation, snowmelt, event-driven discharge (Q_{quick}), seasonal discharge (Q_{slow}), and SPI on NO_3^- concentration, $\delta^{15}\text{N}-\text{NO}_3^-$, and $\delta^{18}\text{O}-\text{NO}_3^-$ at the mountain range scale. Green points are the covariate effects shared among Cascade Range rivers. Purple points are the covariate effects shared among Olympic Mountain rivers. Points are maximum likelihood estimates for each coefficient with horizontal bars indicating the 95% confidence intervals around that estimate.

exports fell (Fig. 3c). While we lack a covariate that adequately captures this seasonal variation, this could be explained by the drainage from a relatively ^{15}N enriched NO_3^- pool, such as septic and manure waste, or by NO_3^- that has undergone denitrification

or biological uptake (assimilation). During denitrification and assimilation, the lighter isotopes of $\delta^{15}\text{N}$ and $\delta^{18}\text{O}$ are preferentially processed, resulting in the dual isotopic enrichment of residual NO_3^- ^{15,35,53,54}. In fact, we do see a shared seasonal enrichment of the $\delta^{15}\text{N}-\text{NO}_3^-$ and $\delta^{18}\text{O}-\text{NO}_3^-$ states in Cascade Range rivers (Fig. 3c, d), suggesting that summertime NO_3^- concentrations could be influenced by nutrient retention processes that occur instream or elsewhere within watersheds. Notably, the Cascade Range watersheds have increased riparian and wetland areas, which promote anoxia and denitrification⁵⁵ (Table 2), and the river channels themselves are conducive to groundwater springs and exchange with the reactive hyporheic zone^{56,57}. As discharge volumes and velocities decline, it is possible that increased connections with biogeochemically reactive sites or increased proportions of denitrified NO_3^- from external pools could seasonally enrich the Cascade Range $\delta^{15}\text{N}-\text{NO}_3^-$ and $\delta^{18}\text{O}-\text{NO}_3^-$ river values^{35,58,59}. However, summertime values of $\delta^{18}\text{O}-\text{NO}_3^-$ across the Cascade Range rivers were distinctly more variable (Fig. 3d) and could also be enriched by unprocessed atmospheric NO_3^- ^{14,60}. Furthermore, processes such as respiration and O-isotopic exchange between NO_2 and H_2O molecules during nitrification can significantly alter $\delta^{18}\text{O}-\text{NO}_3^-$ values³⁶, making nutrient retention patterns difficult to surmise at this regional scale.

In the Olympic Mountain rivers, the observed effects of hydroclimate variables on the isotopic states suggest that NO_3^- concentrations were derived mostly from a combination of soil or instream nitrification processes and contributions from atmospheric deposition. Average $\delta^{15}\text{N}-\text{NO}_3^-$ values were low (Fig. 2), and correlations with seasonal hydroclimate variables were insignificant (Fig. 4c). The lack of significance of $\delta^{15}\text{N}-\text{NO}_3^-$ with temporal variables in Olympic Mountain rivers indicates that $\delta^{15}\text{N}-\text{NO}_3^-$ values were relatively unchanged through time, and there was limited mixing among isotopically distinct sources, or isotopic enrichment from human waste or agricultural inputs. Increased snowmelt in the Olympic Mountains had a positive effect on $\delta^{18}\text{O}-\text{NO}_3^-$, and the singular peak of $\delta^{18}\text{O}-\text{NO}_3^-$ in Olympic Mountain rivers coincided with local climate conditions, rising during a normal hydrologic year in 2016, but absent during 2015, which was a record drought in terms of snowpack for Washington State⁶¹. The positive effect of snowmelt, and the timing of increased $\delta^{18}\text{O}-\text{NO}_3^-$, implies that spring and early summer snowmelt washes unprocessed atmospheric NO_3^- downstream, increasing measurable atmospheric contributions to the Olympic Mountain river NO_3^- pools.

Landform influence on river responses to hydroclimate. The final piece of our analyses identifies watershed-scale differences in landform as a strong underlying control of the contrasting responses of the Cascade Range and Olympic Mountain rivers to hydroclimatic change. We found that a significant amount of the variation in the individual river NO_3^- responses to hydroclimate variables was explained by a simple geomorphic metric, mean watershed slope (Fig. 5). NO_3^- yields, NO_3^- concentrations, and $\delta^{15}\text{N}-\text{NO}_3^-$ values in rivers draining flatter watersheds were distinctly more sensitive to changes in precipitation and storm-event scale flows. In contrast, $\delta^{18}\text{O}-\text{NO}_3^-$ in rivers draining mid- to high-sloped watersheds were less sensitive to runoff-related hydrologic conditions, and highly sensitive to changes in snowmelt (Fig. 5). This relationship between river NO_3^- sensitivities and watershed slope illuminates the broad-scale influence of topography on river ecosystem function. Watershed topography can directly influence the source, transfer, and transport of NO_3^- directly through both physical and chemical mechanisms. For example, in watersheds with steep slopes, strong energy gradients

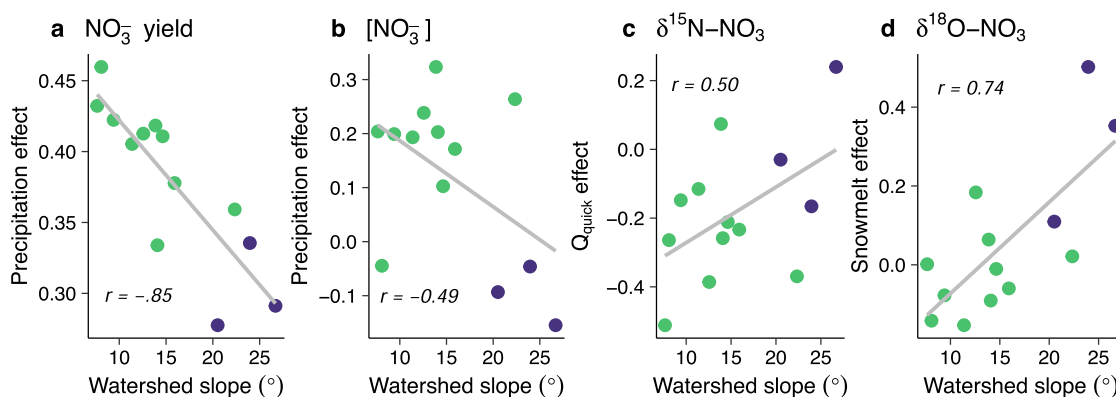


Fig. 5 Watershed-scale MARSS covariate coefficients plotted versus mean watershed slope for each of our best covariate models. a, b Watershed-scale effects of precipitation on NO_3^- yield and NO_3^- concentration plotted versus mean watershed slope. **c** Watershed-scale effects of event-driven discharge (Q_{quick}) on $\delta^{15}\text{N-NO}_3^-$ plotted versus mean watershed slope. **d** Watershed-scale effects of snowmelt on $\delta^{18}\text{O-NO}_3^-$ plotted versus mean watershed slope. Green points represent the covariate effect for each of the Cascade Range rivers. Purple points represent the covariate effect in the Olympic Mountain rivers. Pearson correlation coefficients are given in the lower left or upper left corner of each plot.

rapidly route water and snowmelt to stream channels, quickly transferring available NO_3^- ^{10–12}. Lower relief areas instead increase residence times and rates of N reactivity^{9,11,12}, and also promote river connections to N sources and sinks across high flow (i.e., floodplain soils^{13,62}) and low flow conditions (i.e., hyporheic and channel storage zones^{35,40,58}). Terrain relief can also indirectly affect NO_3^- dynamics through its control on the distribution of human activity. In flat watersheds, humans populate and modify the landscape to larger degrees, enhancing the accumulation of NO_3^- on land and in soils^{16,29}, while often altering hydrologic flow paths⁶³. Together, this can saturate or bypass biogeochemical retention opportunities, and ultimately increase the potential for NO_3^- transfers and transport downstream^{17,64}.

Our results highlight that while regional-scale variation exhibits large controls on monthly NO_3^- sources and exports across the Puget Sound Basin, watershed characteristics still influence river sensitivity to hydroclimate variables. Specifically, our results imply that differences in landform, and therefore availability, source, and transfer of NO_3^- , alters NO_3^- inputs across rivers in the two mountain ranges, as well as the sensitivity of river NO_3^- transport to hydroclimatic change. This finding is similar to recent work from Alaskan watersheds^{11,12,23,26,30,31} and is meaningful in that it supports the notion that watershed slope can act as a master variable for predicting biogeochemical processes, ultimately modifying the response of river ecosystem function to climate. In the Pacific Northwest, climate change is predicted to increase the proportion of precipitation falling as rain relative to snow^{61,65}. With more precipitation falling as rain, instances of flooding and storm-event scale flow are likely to increase, particularly in low and mid-sloped watersheds. The results of our analyses imply that the sensitivity of river NO_3^- transport to hydro-climatic changes may be strongest in watersheds with lower slopes where excess NO_3^- can be stored and remobilized in response to precipitation and high river flows. While further research is needed to understand climate-driven perturbations to river nutrient dynamics across human modified catchments, this work demonstrates the strong influence of topography on river NO_3^- dynamics and reveals watershed slope as a potential predictor of river responses to hydroclimatic change.

Conclusions

This work contributes to the understanding of spatiotemporal patterns of river NO_3^- source and transport, including insight into seasonal patterns, as well as the identification of physical

mechanisms at finer scales. We provide evidence that regional climate exhibits strong controls on monthly isotopic composition, concentration, and yield of river NO_3^- , forming distinct source and transport-driven NO_3^- regimes across two local mountain ranges. Within these broad-scale patterns, we also show that watershed landform influences the availability and transfer of NO_3^- , ultimately controlling the sensitivity of river NO_3^- dynamics to climate. Climate change is likely to have important effects on river NO_3^- transport, with impacts that will play out differently across watersheds^{6,20}. The clear linkage between NO_3^- regimes, hydroclimate, and landform has broad implications for river nutrient management and suggests that topographic features, such as watershed slope, could be used to improve scenarios of NO_3^- transport at the scale of regions, which will become increasingly important as climate, hydrology, and land use continues to change.

Methods

Study area. The Puget Sound basin, located mostly in western Washington State, drains an area of approximately 13,700 km² (Fig. 1). Bounded by the Olympic Mountains to the west and the Cascade Range to the east, watersheds in the basin represent a gradient of geomorphic settings, with lowland and mountain valleys formed by continental glaciers, alpine glaciers, sediment deposition, and incision from rivers⁶⁶. Climate in the basin is seasonally variable, characterized by cool, wet winters, and warm dry summers. The average annual rainfall is 2147 mm, and the average annual air temperature is 8 °C⁶⁷. During the hydrologic years of study, about 1947 and 2478 mm of precipitation fell within 2015 and 2016, respectively, and the average air temperature was 10 °C in 2015 and 9 °C in 2016⁶⁸. For watersheds along both the Cascade and Olympic ranges, about 80% of the annual precipitation occurs from October to March^{67,68}. Within this setting, hydrologic regimes are governed by timing and form of precipitation and are characterized as rainfall-dominated (<600 m elevation with peak discharges in November–February) and mixed rain-and-snow hydrologies (>600 m elevation with peak discharges in February–June)^{66,69}. Groundwater also sustains summer discharge in some rivers, as the unconsolidated glacial sediments of Puget Sound river channels are conducive to springs and hyporheic exchange^{56,57}. Notably, in 2015, substantial winter warming increased the proportion of precipitation falling as rain relative to snow, leading to declines in mountain snowpack and snowmelt-driven spring and summer discharge⁶¹. Though the effects of the

Table 2 River and watershed characteristics of the Puget Sound Basin rivers of study.

River name (Map abbreviation)	Mountain range	NO ₃ ⁻ (mg L ⁻¹)	Stream Order	Watershed area (km ²)	Watershed elevation (m)	Watershed slope (°)	% Urban	% Agriculture	% Wetland	% Forest	Soil Depth (cm)	Soil OM (% by weight)
Deschutes (De)	Cascade	0.75 ± 0.1	3	409	288	8	15.4	8.4	5.0	51.5	139.8	2.2
Samish (Sa)	Cascade	0.74 ± 0.2	4	225	268	8	9.2	7.5	5.8	65.8	143.2	2.4
Green (Gr)	Cascade	0.39 ± 0.2	5	1116	546	11	22.6	4.8	2.4	59.4	140.8	2.2
Nooksack (No)	Cascade	0.33 ± 0.2	5	2046	674	14	4.8	12.4	2.9	62.5	139.3	3.0
Nisqually (Ni)	Cascade	0.25 ± 0.1	5	1853	556	9	8.4	6.4	5.6	59.4	143.8	2.0
Cedar (Ce)	Cascade	0.24 ± 0.1	4	457	611	13	15.8	0.6	1.5	74.1	143.0	1.9
Puyallup (Pu)	Cascade	0.23 ± 0.1	6	2439	921	15	9.1	2.7	2.4	65.9	145.8	1.8
Snohomish (Sro)	Cascade	0.22 ± 0.1	6	4450	688	16	7.1	2.7	2.4	72.1	137.2	1.9
Stillaguamish (St)	Cascade	0.21 ± 0.1	5	1457	604	14	4.3	2.9	1.7	79.3	139.8	2.0
Skagit (Ska)	Cascade	0.09 ± 0.05	6	8035	1128	22	2.0	1.3	0.9	69.7	133.5	2.0
Skokomish (Sko)	Olympic	0.06 ± 0.03	5	592	609	21	5.5	1.0	1.3	72.9	112.6	2.3
Elwha (El)	Olympic	0.03 ± 0.02	4	757	1089	24	0.3	0.0	0.4	81.6	118.3	1.0
Duckabush (Du)	Olympic	0.03 ± 0.02	3	179	1047	27	0.8	0.0	0.3	76.1	95.7	2.0

River and watershed characteristics are ordered by decreasing monthly mean NO₃⁻ concentration. Other descriptors include stream order, watershed area, mean watershed elevation, mean watershed slope, percent urban, agriculture, wetland, and forest cover by area of the watershed, mean watershed soil depth, and mean watershed soil organic matter (OM). Water quality sampling sites are labeled on Figure 1 using the italicized abbreviations in the first column of the table.

snow drought were felt across the entire basin, watersheds in the south Cascade Range and Olympic Mountains experienced the largest impacts to their snowmelt regimes⁶¹.

Land use histories and development in the region have resulted in a gradient of human disturbance and land cover across the basin. While the slopes of the Cascade Range and Olympic Mountains remain mostly forested, transitions to urban and agricultural land uses along with increased logging since the late 1800s have removed substantial areas of floodplain forest in the lower basin. The central Puget Sound region has seen rapid urbanization in recent years, gaining over a million people since 2000⁷⁰. The south and central valleys of the western Cascade Range are now mainly urban and rural residential land, with some pastureland and forage crops (hay and corn) located outside the urban fringe^{71,72}. The majority of forage and specialty crop cultivation (including cereal grains, berries, and vegetables) is located in the northeastern part of the basin in the Nooksack, Skagit and Snohomish river watersheds⁷². Forested areas along the lower Cascade Range are a mix of deciduous and coniferous forest and include large stands of the early successional N-fixing tree species, red alder (*Alnus rubra*)⁷³. Watersheds along the eastern Olympic Mountains remain mostly forested with coniferous trees, but with some logging, and sparse pastureland, forage cropped fields and residential development^{71,72}. The combination of forested, mountainous areas, agricultural valleys, and sprawling cityscapes creates a variable landscape across the Puget Sound basin, and drives a diversity of N inputs that cover the full range of NO₃⁻ sources¹⁵.

Sample and data collection. We used two years of river monthly water quality samples collected by the Washington Department of Ecology’s (DoE) River and Stream Water Quality Monitoring program from October 2014 to September 2016. The Washington DoE collects monthly water quality samples at nearly 100 river and stream stations across Washington state. For this study, we selected rivers that drain the Puget Sound Basin and range in their watershed physical and land use characteristics (Table 2, Fig. 1c). This included 13 rivers, each with 1 DoE sampling station located near the Puget Sound outlet (Fig. 1). River order (i.e., Strahler number⁷⁴) at the mouth ranged from 5 to 8, and sampling stations ranged from 4 to 300 m in elevation. We obtained subsamples of monthly water samples from each river site for NO₃⁻ stable isotope analysis (δ¹⁵N and δ¹⁸O) and paired them with corresponding NO₃⁻ concentration data from the Washington’s Department of Ecology’s Freshwater Information Network database⁷⁵. Details concerning the Washington Department of Ecology’s water quality sample handling protocols and analytical methods can be found in Von Prause, 2021⁷⁶.

To calculate river NO₃⁻ yields, we used the composite method within the loadflex R package⁷⁷ to calculate monthly river NO₃⁻ fluxes (estimated in kg day⁻¹), and subsequently divided monthly fluxes by watershed area for monthly estimates of river NO₃⁻ yield in kg km⁻² day⁻¹. The composite method combines regression model predictions with model residuals to bring predictions closer to actual observations, thereby reducing model biases and increasing the accuracy of total flux estimates⁷⁷⁻⁷⁹. We therefore chose the composite method (in comparison to other methods, such as WRTDS or LOADEST models) as it provided the best estimate of actual river NO₃⁻ yields across our rivers and our period of study. We provide plots of the monthly NO₃⁻ yields, NO₃⁻ concentrations, and NO₃⁻ stable isotopic values (δ¹⁵N and δ¹⁸O) for each river site in Supplementary Figs. 1-4.

Stable isotope analysis of NO₃⁻. We analyzed river water subsamples for nitrogen and oxygen isotope ratios of NO₃⁻ (¹⁵N/¹⁴N

and $^{18}\text{O}/^{16}\text{O}$) using the bacterial denitrifier method^{80,81} at the University of Washington's Δ^* IsoLab. Briefly, we used denitrifying bacteria (*Pseudomonas aureofaciens*) to convert NO_3^- and NO_2 to N_2O . The resultant N_2O was extracted, purified, and pyrolyzed to N_2 and O_2 in a heated gold tube held at 800 °C. The isotopic ratios of each gas were then measured by a Finnigan Delta-Plus Advantage isotope ratio mass spectrometer after being separated by a gas chromatograph. We report the ratios of $^{15}\text{N}/^{14}\text{N}$ and $^{18}\text{O}/^{16}\text{O}$ of NO_3^- in the delta (δ) notation in per mil (‰), where $\delta = (R_{\text{sample}}/R_{\text{standard}} - 1)$ and R is the $^{15}\text{N}/^{14}\text{N}$ in N_2 normalized atmospheric air N_2 (Air) or $^{18}\text{O}/^{16}\text{O}$ normalized to Vienna Standard Mean Ocean Water (VSMOW). We calibrated $\delta^{15}\text{N}$ and $\delta^{18}\text{O}$ of NO_3^- using three international reference materials, USGS34: $\delta^{15}\text{N} = -1.8\text{‰}$, $\delta^{18}\text{O} = -27.8\text{‰}$, USGS35: $\delta^{15}\text{N} = +2.7\text{‰}$, $\delta^{18}\text{O} = +56.8\text{‰}$, and IAEA-NO3: $\delta^{15}\text{N} = +4.7\text{‰}$, $\delta^{18}\text{O} = +25.6\text{‰}$. We verified analytical accuracy using replicate measurements of USGS35 and IAEA-NO3 (for $\delta^{15}\text{N}$ and $\delta^{18}\text{O}$, respectively). The uncertainty was $\pm 0.1\text{‰}$ for $\delta^{15}\text{N}$ and $\pm 0.5\text{‰}$ for $\delta^{18}\text{O}$ (1 SD, $n = 84$).

Regional climate and hydrologic covariates. We considered several climate and hydrologic predictors of river NO_3^- concentration, NO_3^- yield, $\delta^{15}\text{N}-\text{NO}_3^-$, and $\delta^{18}\text{O}-\text{NO}_3^-$ time series. We chose monthly precipitation, snowmelt, water temperature, and the Standardized Precipitation Index (SPI) as metrics of climatic variability. SPI is a widely used drought index which captures how precipitation deviates from the climatological average across different timescales⁸². We used 12-month SPI, which is timescale indicative of long-term drought events⁸². To calculate precipitation and snowmelt values, we extracted gridded estimates of total daily precipitation, and snow water equivalent (SWE) data for each watershed boundary from Oak Ridge National Laboratory's Daymet dataset⁸³ and summed the estimates per each month sampled. We then calculated monthly snowmelt for each watershed as the absolute value of negative differences in the cumulative SWE from each month to the next. We extracted monthly gridded estimates of 12-month SPI for each watershed boundary from the National Oceanic and Atmospheric Administration's nClimGrid-monthly dataset⁸⁴. We obtained monthly water temperature measurements from the Washington's Department of Ecology's Freshwater Information Network database⁷⁵, which were taken in the field alongside the provided river water quality samples.

To evaluate the influence of river hydrologic variation, we included both event-driven and seasonal components of each river's discharge hydrograph. By considering different components of the hydrograph in our analysis, we sought to reveal the role of flashy, runoff-driven flow vs. the sustained, seasonal pulse of river discharge in driving monthly river NO_3^- variation. To calculate seasonal and storm event-scale variations in discharge, we used recession analysis, a method that separates discharge hydrographs into short-term discharge variations driven by surface or interflow during storm events, and baseflow variations driven by slower water transit or eventual groundwater inputs^{85–87}. We extracted daily discharge data from the nearest U.S. Geological Survey gaging station to each study site for the 2 years of study (no greater than 30 km from the sampling point)⁸⁸. To estimate the slow, seasonal (Q_{slow}), and quick, short-term (Q_{quick}) components of the hydrograph, we applied the baseflow recursive filter method^{85,89} to each river hydrograph. To preserve the scale of individual storm events, we kept Q_{quick} as the raw daily value specific to the sample date. To incorporate the influence of river flow at the seasonal scale, we calculated Q_{slow} as the previous week sum of estimated baseflow values. Further details on the estimation and chosen time windows of Q_{quick} and

Q_{slow} can be found in the supplemental material (Supplementary Note 1 and Supplementary Fig. 5).

Watershed and landscape characteristics. We compiled watershed-scale landscape metrics for each of the watersheds corresponding to our 13 river sites using the Environmental Protection Agency's StreamCat data library (Table 2). These metrics included watershed area, mean watershed elevation, mean watershed soil depth, mean soil organic matter, watershed population density, and percent urban, wetland, agricultural, and forested land. We also included mean watershed slope in our analyses as it captures aspects of watershed topography and stream geomorphology that may influence NO_3^- accumulations or transfers, such as water residence times, floodplain area, and hydrologic connectivity^{9,10,12}. We calculated watershed slope as the average of all slope raster pixels within the boundaries of each individual river's watershed using ArcGIS (v10.8).

Time series modeling approach. We used multivariate autoregressive state space (MARSS) models to examine temporal trends in NO_3^- concentration, NO_3^- yield, and NO_3^- isotopic composition ($\delta^{15}\text{N}$ and $\delta^{18}\text{O}$) across 13 major rivers in the Puget Sound basin⁹⁰. MARSS models are a powerful class of time series models that can be used to evaluate hypotheses regarding synchrony among multiple time series^{91–93}. MARSS models consist of two equations. The process Eq. (1) is an estimate of changes in the true, but hidden, states of nature over time. The observation Eq. (2) relates actual observations to the unobservable process Eq. (1).

$$\mathbf{x}_t = \mathbf{B}\mathbf{x}_{t-1} + \mathbf{C}\mathbf{c}_{t-h} + \mathbf{w}_t; \mathbf{w}_t \sim \text{MVN}(\mathbf{0}, \mathbf{Q}) \quad (1)$$

$$\mathbf{y}_t = \mathbf{Z}\mathbf{x}_t + \mathbf{v}_t; \mathbf{v}_t \sim \text{MVN}(\mathbf{0}, \mathbf{R}) \quad (2)$$

In the process model (1), \mathbf{x}_t is a $j \times 1$ vector of hidden states in month t ; j changes with each structure of \mathbf{Z} tested in the observation equation. The $j \times j$ matrix \mathbf{B} contains estimated parameters along the diagonal that determine the degree of mean-reversion of each state process, and zeros elsewhere. The $j \times k$ matrix \mathbf{C} contains the model-estimated effects of environmental covariates measured at time $t - h$, where h represents the time lag between the covariate and the response. The \mathbf{c}_{t-h} vector ($k \times 1$) contains each of the measured hydro-climatic covariate values. The $j \times 1$ vector \mathbf{w}_t contains process errors, which are distributed as a multivariate normal with mean vector $\mathbf{0}$ and covariance matrix \mathbf{Q} . The off-diagonals of the \mathbf{Q} matrix measure covariance in the process errors after accounting for shared trends, thus providing an estimate of independence or correlation between the modeled trends, \mathbf{x}_t .

In the observation model (2), \mathbf{y}_t is an $i \times 1$ vector of measured data (log NO_3^- concentration, log NO_3^- yield, or $\delta^{15}\text{N}$ and $\delta^{18}\text{O}$ of NO_3^-) at time t from each watershed ($i = 13$). The \mathbf{Z} matrix maps each of the measured river time series ($i = 13$) onto the hidden states in \mathbf{x}_t (the term state refers to the true, but unobserved temporal pattern of NO_3^- concentration, yield, or isotopic value). The $i \times 1$ vector \mathbf{v}_t contains the observation errors, which are distributed as a multivariate normal with mean vector $\mathbf{0}$ and covariance matrix \mathbf{R} .

Testing for seasonal patterns in NO_3^- dynamics. By specifying different structures of the \mathbf{Z} matrix, we evaluated the data support for synchrony among NO_3^- concentration, NO_3^- yield, $\delta^{15}\text{N}$ and $\delta^{18}\text{O}$ of NO_3^- time series at different spatial and functional scales ranging from the entire Puget Sound basin to individual watersheds (Table 2). We modeled each response variable separately and tested five options for the \mathbf{Z} matrix, which represented the

following river groupings: (1) all rivers follow the same state (Basin model), (2) there are two states defined by mountain range, one for rivers located in the Cascade Range, and one for rivers located in the Olympic Mountains (Mountain model), (3) there are three states defined by watershed land use (Land use model), (4) there are three states defined by watershed topographic and soil characteristics (Geomorphology model), and (5) each river follows its own independent state or trend through time (Watershed model). To define the Land use and Geomorphology model groupings, we used *k*-means clustering analyses to group the Puget Sound rivers based on the similarity and closeness of their watershed land use and geomorphic characteristics (Table 1 and Supplementary Note 2). To evaluate the possible variance and covariance among state processes, we tested data support for four options of the **Q** matrix including: equal variance and equal covariance, independent variance and independent covariance, independent variance but no covariance, and equal variance but no covariance. Because the collection and laboratory analysis of all samples was the same, we modeled the observation errors as independent and identically distributed (IID), such that **R** had a single estimated value along the diagonal and zeros elsewhere. In this piece of analysis, we set both the **C** and **c** matrices to zero.

Testing covariates as drivers of monthly variation. To evaluate the data support for different climate and hydrologic drivers of temporal variation in NO_3^- concentration, NO_3^- yield, $\delta^{15}\text{N}$ and $\delta^{18}\text{O}$ of NO_3^- , and to test whether the effects of hydroclimate variables were shared across different spatial or functional scales, we used our “Watershed” scale model and adjusted the **C** matrix of the process model (1) to apply the covariate data in the **c** matrix to each watershed state process. We compared models that included 6 potential covariates: water temperature, precipitation, Q_{quick} (as a measure of event-scale discharge), Q_{slow} (as a measure of seasonal-scale baseflow), snowmelt, and SPI. To reduce the number of model parameters, we fit each model with a single covariate, but compared five coefficient or “effect” options. This included (1) a Basin effect where state processes among all rivers responded identically to hydroclimate (one **C** coefficient per covariate); (2) a Mountain range effect where state processes among all rivers in a given mountain range (i.e., Cascade Range vs. Olympic Mountains) responded identically to hydroclimate (**C** = 2); (3) a Land use effect where state processes among rivers that share similar watershed land use responded identically to hydroclimate (**C** = 3); (4) a Geomorphology effect where state processes among rivers that share similar watershed topography and soil characteristics responded identically to hydroclimate (**C** = 3), and (5) a Watershed effect where state processes for each river responded uniquely to hydroclimate (**C** = number of state processes (13); Table 1). To avoid double counting discharge, we did not include discharge (Q_{quick} or Q_{slow}) as a covariate for our NO_3^- yield models.

To facilitate model comparisons and interpretation across river groupings and covariates, we standardized all response variable and covariate data to have a mean of 0 and standard deviation of 1. In our test for spatial synchrony, we used Akaike Information Criterion adjusted for small sample size (AICc)⁹⁴ to rank models with varying numbers of states as determined by the **Z** matrix and different forms of **Q**. In our covariate analysis, we again used AICc to rank different models that varied by which covariate was included (**c** matrix) and the extent to which the effect of the coefficient was shared or unique (**C** matrix). We also included a null “Watershed” model with no covariates. For both analyses, we selected the model with the lowest AICc value as the best model.

We considered models with a ΔAICc of less than 10 to show moderate statistical support.

Post hoc, we used Pearson correlation coefficients to examine if variation in river-specific covariate effect sizes (**C**) could be explained by watershed geomorphic or land use attributes (including watershed area, elevation, slope, soil depth, soil organic matter, and percent urban, wetland, agricultural, and forested land).

Data availability

River nitrate concentration and water temperature data are available through the Washington Department of Ecology Environmental Information System at <http://www.ecology.wa.gov/eim/>. River discharge data can be accessed through the U.S. Geological Survey National Water Information System database at <https://doi.org/10.5066/F7P55KJN>. Climate data (precipitation and SWE) is available through the Oak Ridge National Laboratory Distributed Active Archive Center at <https://doi.org/10.3334/ORNLDAAC/1840>. Standardized precipitation index data can be obtained from the National Oceanic and Atmospheric Administration’s National Centers for Environmental Information at <https://www.ncei.noaa.gov/pub/data/nidis/indices/nclimgrid-monthly/>. River nitrate stable isotope data analyzed in this paper are available at <https://doi.org/10.5061/dryad.76hdr7t36>.

Code availability

The code used in this study has been made publicly available in a GitHub repository and can be accessed from https://github.com/elmstrom/PugetSoundRiver_NO3Iso_MARSS.

Received: 6 February 2023; Accepted: 23 January 2024;

Published online: 20 February 2024

References

- Boyer, E. W. et al. Riverine nitrogen export from the continents to the coasts. *Glob. Biogeochem. Cycles* <https://doi.org/10.1029/2005GB002537> (2006).
- Galloway, J. N. et al. Nitrogen cycles: past, present, and future. *Biogeochemistry* **70**, 153–226 (2004).
- Howarth, R. W. & Marino, R. Nitrogen as the limiting nutrient for eutrophication in coastal marine ecosystems: evolving views over three decades. *Limnol. Oceanogr.* **51**, 364–376 (2006).
- Vitousek, P. M. et al. Human alteration of the global nitrogen cycle: sources and consequences. *Ecol. Appl.* **7**, 737–750 (1997).
- Battye, W., Aneja, V. P. & Schlesinger, W. H. Is nitrogen the next carbon? *Earths Future* **5**, 894–904 (2017).
- Sinha, E., Michalak, A. M. & Balaji, V. Eutrophication will increase during the 21st century as a result of precipitation changes. *Science* **357**, 405–408 (2017).
- Lewis, D. B. & Grimm, N. B. Hierarchical regulation of nitrogen export from urban catchments: interactions of storms and landscapes. *Ecol. Appl.* **17**, 2347–2364 (2007).
- Howarth, R. et al. Nitrogen fluxes from the landscape are controlled by net anthropogenic nitrogen inputs and by climate. *Front. Ecol. Environ.* **10**, 37–43 (2012).
- Goyette, J.-O., Bennett, E. M. & Maranger, R. Differential influence of landscape features and climate on nitrogen and phosphorus transport throughout the watershed. *Biogeochemistry* **142**, 155–174 (2019).
- Schiff, S. L. et al. Two adjacent forested catchments: dramatically different NO_3^- export. *Water Resour. Res.* **38**, 28-1–28-13 (2002).
- Harms, T. K. et al. Catchment influence on nitrate and dissolved organic matter in Alaskan streams across a latitudinal gradient. *J. Geophys. Res. Biogeosci.* **121**, 350–369 (2016).
- Connolly, C. T. et al. Watershed slope as a predictor of fluvial dissolved organic matter and nitrate concentrations across geographical space and catchment size in the Arctic. *Environ. Res. Lett.* **13**, 104015 (2018).
- Noe, G. B. & Hupp, C. R. Seasonal variation in nutrient retention during inundation of a short-hydroperiod floodplain. *River Res. Appl.* **23**, 1088–1101 (2007).
- Bourgeois, I. et al. Atmospheric nitrate export in streams along a montane to urban gradient. *Sci. Total Environ.* **633**, 329–340 (2018).
- Kendall, C., Elliott, E. M. & Wankel, S. D. In *Stable Isotopes in Ecology and Environmental Science* (eds. Michener, R. & Lajtha, K.) 375–449 (Blackwell Publishing Ltd, 2007).
- Van Meter, K. J., Basu, N. B., Veenstra, J. J. & Burras, C. L. The nitrogen legacy: emerging evidence of nitrogen accumulation in anthropogenic landscapes. *Environ. Res. Lett.* **11**, 035014 (2016).

17. Kumar, P. et al. Critical transition in critical zone of intensively managed landscapes. *Anthropocene* **22**, 10–19 (2018).
18. Compton, J. E., Goodwin, K. E., Sobota, D. J. & Lin, J. Seasonal disconnect between streamflow and retention shapes riverine nitrogen export in the Willamette River Basin, Oregon. *Ecosystems* **23**, 1–17 (2020).
19. Sinha, E. & Michalak, A. M. Precipitation dominates interannual variability of riverine nitrogen loading across the continental United States. *Environ. Sci. Technol.* **50**, 12874–12884 (2016).
20. Soranno, P. A. et al. Spatial and temporal variation of ecosystem properties at macroscales. *Ecol. Lett.* **22**, 1587–1598 (2019).
21. Heffernan, J. B. et al. Macrosystems ecology: understanding ecological patterns and processes at continental scales. *Front. Ecol. Environ.* **12**, 5–14 (2014).
22. Levin, S. A. The problem of pattern and scale in ecology: The Robert H. MacArthur Award Lecture. *Ecology* **73**, 1943–1967 (1992).
23. Smits, A. P., Schindler, D. E., Holtgrieve, G. W., Jankowski, K. J. & French, D. W. Watershed geomorphology interacts with precipitation to influence the magnitude and source of CO₂ emissions from Alaskan streams. *J. Geophys. Res. Biogeosci.* **122**, 1903–1921 (2017).
24. Poff, N. L. In *Global Climate Change and Freshwater Ecosystems* (eds. Firth, P. & Fisher, S. G.) 88–115 (Springer, 1992).
25. Mauger, G. S. et al. *State of Knowledge: Climate Change in Puget Sound. Encyclopedia of Puget Sound* (University of Washington, 2015).
26. Jankowski, K. J. & Schindler, D. E. Watershed geomorphology modifies the sensitivity of aquatic ecosystem metabolism to temperature. *Sci. Rep.* **9**, 17619 (2019).
27. McCluney, K. E. et al. Riverine macrosystems ecology: sensitivity, resistance, and resilience of whole river basins with human alterations. *Front. Ecol. Environ.* **12**, 48–58 (2014).
28. Van Meter, K. J., Chowdhury, S., Byrnes, D. K. & Basu, N. B. Biogeochemical asynchrony: ecosystem drivers of seasonal concentration regimes across the Great Lakes Basin. *Limnol. Oceanogr.* **65**, 848–862 (2020).
29. Basu, N. B. et al. Nutrient loads exported from managed catchments reveal emergent biogeochemical stationarity. *Geophys. Res. Lett.* <https://doi.org/10.1029/2010GL045168> (2010).
30. Lisi, P. J., Schindler, D. E., Cline, T. J., Scheuerell, M. D. & Walsh, P. B. Watershed geomorphology and snowmelt control stream thermal sensitivity to air temperature. *Geophys. Res. Lett.* **42**, 3380–3388 (2015).
31. Cline, T. J., Schindler, D. E., Walsworth, T. E., French, D. W. & Lisi, P. J. Low snowpack reduces thermal response diversity among streams across a landscape. *Limnol. Oceanogr. Lett.* **5**, 254–263 (2020).
32. Holtgrieve, G. W., Schindler, D. E., Gowell, C. P., Ruff, C. P. & Lisi, P. J. Stream geomorphology regulates the effects on periphyton of ecosystem engineering and nutrient enrichment by Pacific salmon. *Freshw. Biol.* **55**, 2598–2611 (2010).
33. Lottig, N. R. et al. Macroscale patterns of synchrony identify complex relationships among spatial and temporal ecosystem drivers. *Ecosphere* **8**, e02024 (2017).
34. Matiatos, I. et al. Global patterns of nitrate isotope composition in rivers and adjacent aquifers reveal reactive nitrogen cascading. *Commun. Earth Environ.* **2**, 1–10 (2021).
35. Briand, C. et al. Legacy of contaminant N sources to the NO₃[−] signature in rivers: a combined isotopic ($\delta^{15}\text{N-NO}_3^-$, $\delta^{18}\text{O-NO}_3^-$, $\delta^{11}\text{B}$) and microbiological investigation. *Sci. Rep.* **7**, 41703 (2017).
36. Venkiteswaran, J. J., Boeckx, P. & Goody, D. C. Towards a global interpretation of dual nitrate isotopes in surface waters. *J. Hydrol. X* **4**, 100037 (2019).
37. Rollinson, V. R. et al. Seasonality of nitrogen sources, cycling, and loading in a New England river discerned from nitrate isotope ratios. *Biogeosciences* **18**, 3421–3444 (2021).
38. Wadnerkar, P. D. et al. Land use and episodic rainfall as drivers of nitrogen exports in subtropical rivers: insights from $\delta^{15}\text{N-NO}_3^-$, $\delta^{18}\text{O-NO}_3^-$ and ^{222}Rn . *Sci. Total Environ.* **758**, 143669 (2021).
39. Chen, F., Jia, G. & Chen, J. Nitrate sources and watershed denitrification inferred from nitrate dual isotopes in the Beijing River, south China. *Biogeochemistry* **94**, 163–174 (2009).
40. Lohse, K. A., Sanderman, J. & Amundson, R. Identifying sources and processes influencing nitrogen export to a small stream using dual isotopes of nitrate. *Water Resour. Res.* **49**, 5715–5731 (2013).
41. Jiang, H., Liu, W., Li, Y., Zhang, J. & Xu, Z. Multiple isotopes reveal a hydrology dominated control on the nitrogen cycling in the Nuijiang River Basin, the last undammed large river basin on the Tibetan Plateau. *Environ. Sci. Technol.* **56**, 4610–4619 (2022).
42. Bourgeois, I. et al. Tracing the fate of atmospheric nitrate in a subalpine watershed using $\Delta 17\text{O}$. *Environ. Sci. Technol.* **52**, 5561–5570 (2018).
43. Jankowski, K., Schindler, D. E. & Holtgrieve, G. W. Assessing nonpoint-source nitrogen loading and nitrogen fixation in lakes using $\delta^{15}\text{N}$ and nitrogen stoichiometry. *Limnol. Oceanogr.* **57**, 671–683 (2012).
44. Weitzman, J. N., Brooks, J. R., Mayer, P. M., Rugh, W. D. & Compton, J. E. Coupling the dual isotopes of water ($\delta^2\text{H}$ and $\delta^{18}\text{O}$) and nitrate ($\delta^{15}\text{N}$ and $\delta^{18}\text{O}$): a new framework for classifying current and legacy groundwater pollution. *Environ. Res. Lett.* **16**, 045008 (2011).
45. Compton, J. E., Church, M. R., Larned, S. T. & Hogsett, W. E. Nitrogen export from forested watersheds in the Oregon coast range: the role of N₂-fixing red alder. *Ecosystems* **6**, 773–785 (2003).
46. Hundey, E. J., Russell, S. D., Longstaffe, F. J. & Moser, K. A. Agriculture causes nitrate fertilization of remote alpine lakes. *Nat. Commun.* **7**, 10571 (2016).
47. Duncan, J. M., Band, L. E. & Groffman, P. M. Variable nitrate concentration–discharge relationships in a forested watershed. *Hydrol. Process.* **31**, 1817–1824 (2017).
48. Goodale, C. L. et al. Unusual seasonal patterns and inferred processes of nitrogen retention in forested headwaters of the Upper Susquehanna River. *Biogeochemistry* **93**, 197–218 (2009).
49. Sebilo, M., Mayer, B., Nicolardot, B., Pinay, G. & Mariotti, A. Long-term fate of nitrate fertilizer in agricultural soils. *Proc. Natl Acad. Sci. USA* **110**, 18185–18189 (2013).
50. Lin, X. et al. Discriminating surface soil inorganic nitrogen cycling under various land uses in a watershed with simulations of energy balanced temperature and slope introduced moisture. *J. Hydrol.* **587**, 124950 (2020).
51. Perakis, S. S., Matkins, J. J. & Hibbs, D. E. N₂-fixing red alder indirectly accelerates ecosystem nitrogen cycling. *Ecosystems* **15**, 1182–1193 (2012).
52. Hart, S. C., Binkley, D. & Perry, D. A. Influence of red alder on soil nitrogen transformations in two conifer forests of contrasting productivity. *Soil Biol. Biochem.* **29**, 1111–1123 (1997).
53. Aravena, R. & Robertson, W. D. Use of multiple isotope tracers to evaluate denitrification in ground water: study of nitrate from a large-flux septic system plume. *Groundwater* **36**, 975–982 (1998).
54. Böttcher, J., Strebel, O., Voerkelius, S. & Schmidt, H.-L. Using isotope fractionation of nitrate-nitrogen and nitrate-oxygen for evaluation of microbial denitrification in a sandy aquifer. *J. Hydrol.* **114**, 413–424 (1990).
55. Hanson, G. C., Groffman, P. M. & Gold, A. J. Denitrification in Riparian wetlands receiving high and low groundwater nitrate inputs. *J. Environ. Qual.* **23**, 917–922 (1994).
56. McGill, L. M., Brooks, J. R. & Steel, E. A. Spatiotemporal dynamics of water sources in a mountain river basin inferred through $\delta^2\text{H}$ and $\delta^{18}\text{O}$ of water. *Hydrol. Process.* **35**, e14063 (2021).
57. Booth, D. B., Haugerud, R. A. & Goetz Troost, K. In *Restoration of Puget Sound Rivers* (eds. Montgomery, D. R., Bolton, S., Booth, D. B. & Wall, L.) 14–45 (University of Washington Press, 2003).
58. Marcé, R., von Schiller, D., Aguilera, R., Martí, E. & Bernal, S. Contribution of hydrologic opportunity and biogeochemical reactivity to the variability of nutrient retention in river networks. *Glob. Biogeochem. Cycles* **32**, 376–388 (2018).
59. Gomez-Velez, J. D., Harvey, J. W., Cardenas, M. B. & Kiel, B. Denitrification in the Mississippi River network controlled by flow through river bedforms. *Nat. Geosci.* **8**, 941–945 (2015).
60. Bostic, J. T., Nelson, D. M., Sabo, R. D. & Eshleman, K. N. Terrestrial nitrogen inputs affect the export of unprocessed atmospheric nitrate to surface waters: insights from triple oxygen isotopes of nitrate. *Ecosystems* **25**, 1384–1399 (2022).
61. Marlier, M. E. et al. The 2015 drought in Washington State: a harbinger of things to come? *Environ. Res. Lett.* **12**, 114008 (2017).
62. Bechtold, J. S., Edwards, R. T. & Naiman, R. J. Biotic versus hydrologic control over seasonal nitrate leaching in a floodplain forest. *Biogeochemistry* **63**, 53–72 (2003).
63. Kaushal, S. S. et al. Land use and climate variability amplify carbon, nutrient, and contaminant pulses: a review with management implications. *J. Am. Water Resour. Assoc.* **50**, 585–614 (2014).
64. Mulholland, P. J. et al. Stream denitrification across biomes and its response to anthropogenic nitrate loading. *Nature* **452**, 202–205 (2008).
65. Hamlet, A. F. et al. An overview of the Columbia basin climate change scenarios project: approach, methods, and summary of key results. *Atmos. Ocean* **51**, 392–415 (2013).
66. Hall, J. E. et al. Large river habitat complexity and productivity of Puget Sound Chinook salmon. *PLoS ONE* **13**, e0205127 (2018).
67. PRISM Climate Group. PRISM gridded climate data: 30-year normal precipitation (period 1981–2010). <http://prism.oregonstate.edu/normal/> (2015).
68. PRISM Climate Group. PRISM gridded climate data: recent years (January 1981 - March 2023). <http://prism.oregonstate.edu/recent/> (2023).
69. Reidy Liermann, C. A. et al. Hydrogeomorphic classification of Washington state rivers to support emerging environmental flow management strategies. *River Res. Appl.* **28**, 1340–1358 (2012).
70. Puget Sound Regional Council. Regional data profile: population and households. <https://www.psrc.org/rdp-population> (2017).

71. Hill, R. A., Weber, M. H., Leibowitz, S. G., Olsen, A. R. & Thornbrugh, D. J. The Stream-Catchment (StreamCat) Dataset: a database of watershed metrics for the conterminous United States. *J. Am. Water Resour. Assoc.* **52**, 120–128 (2016).
72. WSDA (Washington State Department of Agriculture). 2015 WSDA agricultural land use. <https://agr.wa.gov/departments/land-and-water/natural-resources/agricultural-land-use> (2022).
73. Wise, D. R. & Johnson, H. M. Surface-water nutrient conditions and sources in the United States Pacific Northwest. *J. Am. Water Resour. Assoc.* **47**, 1110–1135 (2011).
74. Strahler, A. N. Hypsometric (area-altitude) analysis of erosional topography. *GSA Bull.* **63**, 1117–1142 (1952).
75. Washington Department of Ecology. Environmental information management system. AMS001. <http://www.ecology.wa.gov/eim/> (2019).
76. Von Prause, M. Quality assurance monitoring plan: statewide river and stream ambient water quality monitoring. Publication 21–03-109. Washington State Department of Ecology, Olympia. <https://apps.ecology.wa.gov/publications/SummaryPages/2103109.html> (2021).
77. Appling, A. P., Leon, M. C. & McDowell, W. H. Reducing bias and quantifying uncertainty in watershed flux estimates: the R package loadflex. *Ecosphere* **6**, 1–25 (2015).
78. Aulenbach, B. T. & Hooper, R. P. The composite method: an improved method for stream-water solute load estimation. *Hydrol. Process.* **20**, 3029–3047 (2006).
79. Aulenbach, B. T. Improving regression-model-based streamwater constituent load estimates derived from serially correlated data. *J. Hydrol.* **503**, 55–66 (2013).
80. Sigman, D. M. et al. A bacterial method for the nitrogen isotopic analysis of nitrate in seawater and freshwater. *Anal. Chem.* **73**, 4145–4153 (2001).
81. Kaiser, J., Hastings, M. G., Houlton, B. Z., Röckmann, T. & Sigman, D. M. Triple oxygen isotope analysis of nitrate using the denitrifier method and thermal decomposition of N₂O. *Anal. Chem.* **79**, 599–607 (2007).
82. Zargar, A., Sadiq, R., Naser, B. & Khan, F. I. A review of drought indices. *Environ. Rev.* **19**, 333–349 (2011).
83. Thornton, M. M. et al. Daymet: daily surface weather data on a 1-km grid for North America, Version 4. ORNL DAAC. <https://doi.org/10.3334/ORNLDAAC/1840> (2020).
84. NOAA National Centers for Environmental Information. U.S. Gridded Standardized Precipitation Index (SPI) from nClimGrid-Monthly. <https://www.drought.gov/data-maps-tools/us-gridded-standardized-precipitation-index-spi-nclimgrid-monthly> (2023).
85. Nathan, R. J. & McMahon, T. A. Evaluation of automated techniques for base flow and recession analyses. *Water Resour. Res.* **26**, 1465–1473 (1990).
86. Xie, J. et al. Evaluation of typical methods for baseflow separation in the contiguous United States. *J. Hydrol.* **583**, 124628 (2020).
87. Lyne, V. & Hollick, M. Stochastic time-variable rainfall-runoff modelling. In *Institute of Engineers Australian National Conference*, Publication No 79/10, 89–92 (1979).
88. U.S. Geological Survey [USGS]. USGS water data for the Nation: U.S. Geological Survey National Water Information System database. <https://doi.org/10.5066/F7P55KJN> (2022).
89. Minaudo, C. et al. Seasonal and event-based concentration-discharge relationships to identify catchment controls on nutrient export regimes. *Adv. Water Resour.* **131**, 103379 (2019).
90. Holmes, W., Eric J. & Scheuerell, M. D. Analysis of multivariate time series using the MARSS package. Version 3.11.4. <https://doi.org/10.5281/ZENODO.5781847> (2021).
91. Jankowski, K. J., Houser, J. N., Scheuerell, M. D. & Smits, A. P. Warmer winters increase the biomass of phytoplankton in a large floodplain river. *J. Geophys. Res. Biogeosci.* **126**, e2020JG006135 (2021).
92. Smits, A. P. et al. Detecting signals of large-scale climate phenomena in discharge and nutrient loads in the Mississippi-Atchafalaya river basin. *Geophys. Res. Lett.* **46**, 3791–3801 (2019).
93. Webster, A. J., Douglas, T. A., Regier, P., Scheuerell, M. D. & Harms, T. K. Multi-scale temporal patterns in stream biogeochemistry indicate linked permafrost and ecological dynamics of boreal catchments. *Ecosystems* **25**, 1189–1206 (2022).
94. Burnham, P. K. & Anderson, D. R. (eds.) *Model Selection and Multimodel Inference*. (Springer, 2004).

Acknowledgements

We are deeply indebted to the Washington Department of Ecology for providing the water samples used for the nitrate stable isotope analysis. Additionally, we thank Dr. Kathi Jo Jankowski, Dr. Lillian McGill, and Dr. Sydney Clark for their assistance with the statistical and laboratory analyses. This research was partially funded by a Department of the Interior Northwest Climate Adaptation Science Center graduate fellowship and a National Oceanic and Atmospheric Administration Margaret A. Davidson graduate fellowship awarded to E.J.E. The H. Mason Keeler Endowed Professorship, the H. Mason Keeler Endowment for Excellence, and the Future Rivers program at the University of Washington through the NSF National Research Traineeship award (DGE 1922004) provided additional support to G.W.H. and E.J.E. Any use of trade, firm, or product names is for descriptive purposes only and does not imply endorsement by the U.S. Government.

Author contributions

G.W.H. and E.J.E. conceived the study. A.J.S. designed, built, and maintained the laboratory setup. E.J.E., A.J.S., and K.L. conducted the laboratory analysis. E.J.E. undertook the formal data analysis and visualization of the work. M.D.S. contributed to the data analysis and code. G.W.H., E.J.E., and M.D.S. discussed and interpreted the results. E.J.E. wrote the original draft of the manuscript, which was then refined and edited by all authors.

Competing interests

The authors declare no competing interests.

Additional information

Supplementary information The online version contains supplementary material available at <https://doi.org/10.1038/s43247-024-01235-8>.

Correspondence and requests for materials should be addressed to Elizabeth J. Elmstrom.

Peer review information *Communications Earth & Environment* thanks Nina Welti and the other, anonymous, reviewer(s) for their contribution to the peer review of this work. Primary handling editors: Joshua Dean, Clare Davis and Martina Grecequet. A peer review file is available.

Reprints and permission information is available at <http://www.nature.com/reprints>

Publisher's note Springer Nature remains neutral with regard to jurisdictional claims in published maps and institutional affiliations.



Open Access This article is licensed under a Creative Commons

Attribution 4.0 International License, which permits use, sharing, adaptation, distribution and reproduction in any medium or format, as long as you give appropriate credit to the original author(s) and the source, provide a link to the Creative Commons license, and indicate if changes were made. The images or other third party material in this article are included in the article's Creative Commons license, unless indicated otherwise in a credit line to the material. If material is not included in the article's Creative Commons license and your intended use is not permitted by statutory regulation or exceeds the permitted use, you will need to obtain permission directly from the copyright holder. To view a copy of this license, visit <http://creativecommons.org/licenses/by/4.0/>.

© The Author(s) 2024